Detailed design of imaging bolometer fields of view for Wendelstein7-X

B. J. Peterson[1,2], R. Sano[3], D. Zhang[4], Y. Feng[4], K. Mukai[1,2],
M. Jakubowski[4], M. Krychowiak[4], R. Koenig[4], T. Sunn Pedersen[4]

[1] *National Institute for Fusion Science, Toki, Japan*

[2] *Grad. Univ. for Advanced Studies (SOKENDAI) , Toki, Japan*

[3] *National Institutes for Quantum and Radiological Science and Technology, Naka, Japan*

[4] *Max-Planck-Institute for Plasma Physics, Greifswald, Germany*

Abstract

The fields of view of four imaging bolometers for Wendelstein 7-X are designed for two different IR cameras resulting in imaging bolometers with 18 x 24 (30 x 40) pixels and a time resolution of 33 (20) ms. Estimates of the signal strength based both on a simple assumption of uniformly radiating plasma and on synthetic images based on the results of an edge impurity transport model are compared with the calculated noise equivalent power giving adequate signal to noise ratios ranging from 40 to 890. Comparison of synthetic images shows the advantages of the advanced IR camera in resolving finer radiation structures through higher resolution and the ability of the IRVBs to measure changes in radiation structure due to detachment.

I. Introduction

The InfraRed imaging Video Bolometer (IRVB) [1] is a diagnostic which provides absolutely calibrated images of total (wavelength integrated) radiation from a plasma by solving the heat diffusion equation of a thin (2 μm) 9 cm x 7 cm Pt foil blackened with graphite, which is exposed to the plasma radiation through an aperture in a pinhole camera arrangement. The resulting temperature distribution on the foil is measured from the side opposite the plasma radiation using an IR camera located outside the vacuum vessel. In this paper we present the detailed designs of the fields of view (FoV) of four imaging bolometers that view the divertor and non-divertor regions of the Wendelstein 7-X (W7-X) [2] plasma. The objective of these IRVBs is to take advantage of the two dimensional (2D) imaging to observe the complex radiation patterns from the three dimensional (3D) divertor (including radiation from plasma wall interaction) and non-divertor plasma regions of W7-X. The images from these IRVBs can then be directly and quantitatively compared with the synthetic images generated from the IRVB geometry and the results of a 3D impurity modelling code

such as EMC3-EIRENE [3]. By modifying the model assumptions to obtain better agreement with the experimental images, insight into the physics of impurity transport can be gained.

II. Imaging bolometer parameters

These designs, for comparison, assume two different IR camera specifications: one using a long wavelength (8-12 μm) microbolometer detector (640 x 480 pixel, 30 fps, 100 mK) and the other (following parameters are given in {}) using a midwavelength (3-5 μm) InSb detector (1280 x 1024 pixel, 105 fps, 40 mK). The 8 cm x 6 cm central section of the foil is located a distance $l_{ap\text{-}f}$ (see Table 1) from an aperture of area A_{ap} = 4.3 x 4.3 {2.6 x 2.6} mm^2 and is divided into N_{bol} = *18 x 24 {30 x 40}* IRVB channels, each consisting of 504 {791} IR camera pixels. The locations of the four IRVBs in W7-X are indicated in Table 1 and are detailed elsewhere [4].

Table 1 IRVB design parameters

Port	divertor region viewed	IRVB	$l_{ap\text{-}f}$ (cm)	S_{signal} (Eq. 2) (W/m^2)	SNR	S_{signal} (C_{rad}=.4) (W/m^2)	SNR	S_{signal} (C_{rad}=.9) (W/m^2)	SNR
AEM 30	high ι	A	7.5	52 {19}	47 {45}	58 {21}	53 {51}	470 {148}	429 {359}
	none	B	6	81 {29}	74 {71}	667 {366}	609 {889}	651 {330}	595 {802}
AEA 41	low ι	C	8	45 {16}	42 {40}	121 {41}	111 {100}	261 {109}	238 {265}
	none	D	7	59 {21}	54 {52}	347 {226}	317 {549}	173 {126}	158 {306}

Using Equation 1, the noise equivalent power density (NEPD), S_{IRVB}, of the IRVBs is calculated as 1.09 W/m^2 {0.41 W/m^2}

$$S_{IRVB} = \frac{\eta_{IRVB} N_{bol}}{A_f} = \frac{\sqrt{10} k t_f \sigma_{IR}}{\sqrt{f_{IR} N_{IR}}} \sqrt{\frac{N_{bol}^3 f_{bol}}{A_f^2} + \frac{N_{bol} f_{bol}^3}{5\kappa^2}} \quad (1)$$

$$S_{signal} = \frac{P_{signal}}{A_{bol}} = \frac{A_{bol} A_{ap} \cos^4 \vartheta P_{rad} l_{plasma}}{A_{bol} 4\pi l_{ap-f}^2 V_{plasma}} \quad (2)$$

where η_{IRVB} is the IRVB noise equivalent power, A_f = *48* cm^2 is the utilized area of the foil, k = *0.716* W/cmK is the thermal conductivity of the foil, t_f = *2 μm* is the thickness of the foil, f_{IR} = *30 {105}* fps is the frame rate of the IR camera, N_{IR} is the number of IR camera pixels

used, $f_{bol} = 30$ {*50*} fps is the frame rate of the IRVB and $\kappa = 0.251$ cm^2/s is the foil thermal diffusivity. Equation 1 is derived from Eq. 10 in Ref. [1] by dividing η_{IRVB} by the area of each bolometer channel, $A_{bol} = A_f/N_{bol} = 11.1$ {*4.0*} mm^2 and neglecting the contribution of the black body radiation term. The signal level is estimated from Equation 2 and shown in Table 1 where P_{signal} is the radiated power to each detector from the plasma, $A_{ap} = 18.8$ {*6.8*} mm^2 is the area of the aperture, $P_{rad} = 5$ MW is the total power radiated by the plasma, $V_{plasma} = 30$ m^3 is the volume of the plasma $l_{plasma} = 150$ cm is the average path length of the sightline through the plasma, and $\theta = 20^\circ$ is the average angle of each detector's line of sight with respect to the aperture normal vector for a time resolution ($1/f_{bol}$) of 33 {20} ms. The signal to noise ratio (SNR) is calculated by dividing Equation 2 by Equation 1 and the results are also shown in Table 1.

III. Synthetic images

Using EMC3-EIRENE [3] data for the 3D carbon radiation distribution in the scrape off layer (SOL) and the response/geometry matrices for the individual IRVBs (which depend on their viewing geometries) synthetic images of the radiated power density absorbed by the IRVB foil are calculated [5] as shown in Figure 1. The EMC3-EIRENE input parameters are 10 MW of power entering the SOL, a total carbon SOL radiation fraction of $C_{rad} = 0.4$ (attached) and 0.9 (detached). The magnetic configuration is the standard divertor configuration with full island control current of 25 kA. The synthetic images also gives a more accurate and channel-specific estimate of the signal levels for SNR estimates, the maximum values of which are shown in Table 1.

IV. Discussion and Conclusion

This work demonstrates that IRVBs with reasonable FoVs, sensitivity and spatial resolution can be designed as tools to diagnose radiative structures in W7-X. In particular, transitions in the radiation structure going from attachment to detachment are evident in the changes between Figures 1 (B3) and (B4) and between (C3) and (C4), respectively. The advantages of the higher performance IR camera are seen in its ability to resolve finer radiation structures (compare Figures 1(C1) and (C3)) due to higher spatial resolution. In the future, the IRVBs FoVs can be optimized by using the synthetic images as a guide to the more relevant regions of higher radiation intensity.

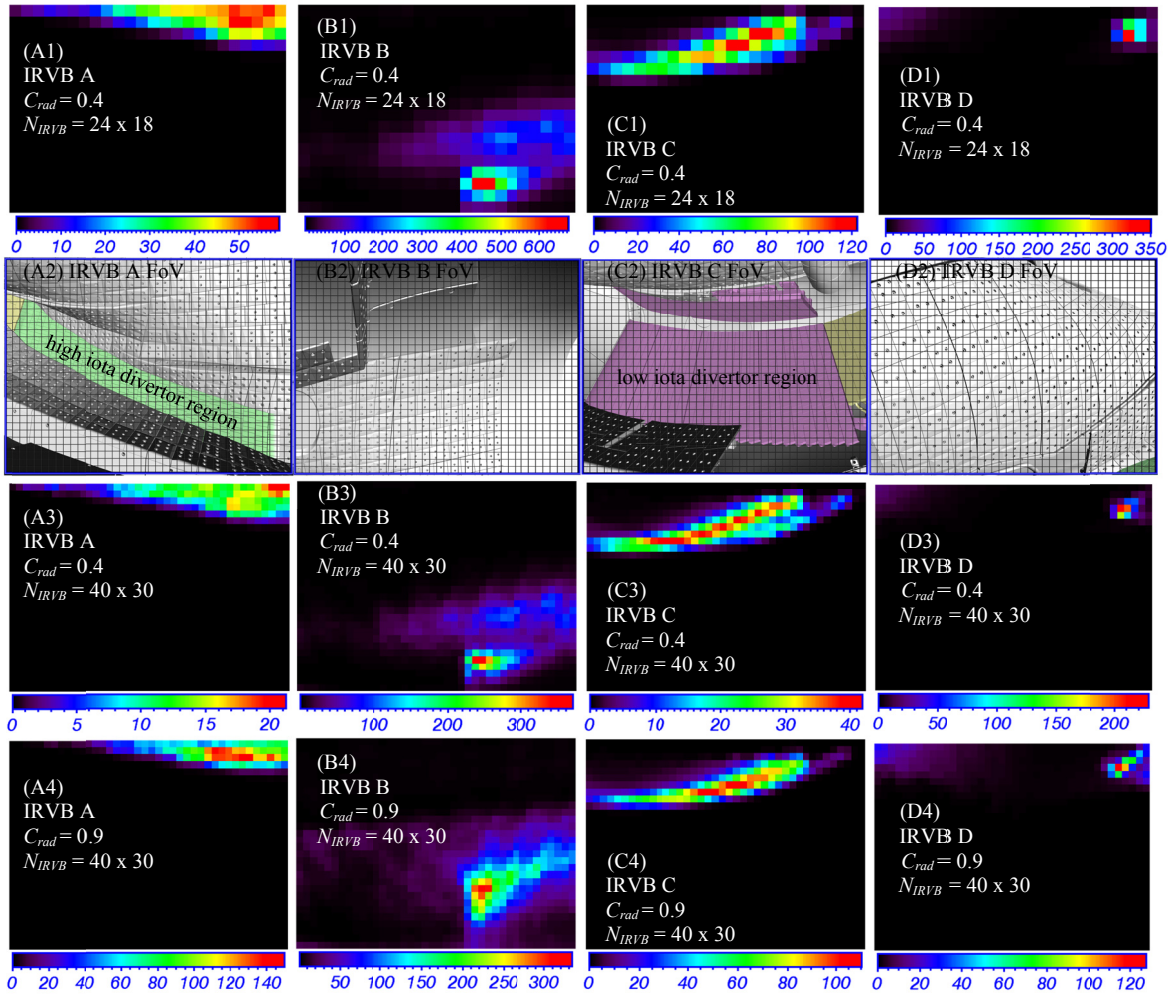

Fig. 1 CAD images of FoVs for IRVBs (with 30 x 40 pixels) in W7-X (row 2) and synthetic images of carbon radiated power (W/m^2) for IRVBs A, B, C and D for N_{IRVB} = 24 x 18 and C_{rad} = 0.4 (row 1) and for N_{IRVB} = 40 x 30 and C_{rad} = 0.4 (row 3) and C_{rad} = 0.9 (row 4).

Acknowledgement

The authors acknowledge support from the National Institute for Fusion Science (Japan) budget NIFS15ULHH026.

References

[1] B. J. Peterson et al., Rev. Sci. Instrum. **74** (2003) 2040.

[2] T. Klinger et al, Fus. Eng. Design **88** (2013) 461.

[3] Y. Feng et al., Plasma Phys. Contr. Fusion **44** (2002) 611

[4] B. J. Peterson et al., Plasma Fus. Res. **11** (2016) 2402101.

[5] B. J. Peterson et al., Plasma Fus. Res. **8** (2013) 2402037.